Supporting Information

Electric and magnetic field-induced birefringence of 2D nanocolloidal liquid crystals with large magneto–optical Kerr effect

*Huai-Ke Jia[1], Zhe Song[1], Yu-Yang Su[1], Zhao-Qing Wang[1] , Xiao-Song Li[1] and Tian-Zi Shen[1]**

[1] School of Instrumentation and Optoelectronic Engineering, Beihang University, Beijing, 100191,PR China.

Note: Sensitivity of 2D LCs to electric/magnetic fields

The sensitivity of 2D LCs to electric and magnetic fields is analyzed using the Kerr and Cotton–Mouton (CM) coefficients[1, 2]. Theoretically, the birefringence curves in these fields follow a Langevin function, where the birefringence is linearly related to the square of the field strength[3, 4], expressed as

$$\Delta n_E = K\lambda E^2, \quad \text{(S1)}$$

$$\Delta n_B = C\lambda B^2, \quad \text{(S2)}$$

Where K and C denote the Kerr and CM coefficients, respectively, these two equations are valid only under a small field because of the higher-order terms involved under stronger fields. Using Equations S1-2, we determined that 2D LCs exhibit their largest Kerr coefficient at the concentration of 0.3 wt%, calculated to be 1.5×10^{-6} mV^{-2}. At this concentration, the CM coefficient is approximately 54 $T^{-2}m^{-1}$. However, as the concentration increases to 0.6 wt%, the CM coefficients rise to a maximum of 1.8×10^{2} $T^{-2}m^{-1}$, whereas the Kerr coefficient gradually decreases to 0.

By taking the inverse of E^2 and B^2, the Δn_{sat} can be obtained. Using the experimental data on Δn and Δn_{sat} of the 2D LC, we can estimate the anisotropy of polarizability as

$$\Delta\alpha = \frac{15k_BT\Delta n_E}{\Delta n_{sat}\varphi E^2}. \quad \text{(S3)}$$

Where φ denotes the volume ratio. Thus, using Equation S3, the value of $\Delta\alpha$ was estimated to be -7.7×10^{-22} Fm^2. By contrast, the field-induced magnetic susceptibility $\Delta\chi$ is expressed as

$$\Delta\chi = \frac{15k_BT\Delta n_B}{\Delta n_{sat}\varphi B^2} \quad \text{(S4)}$$

Using Equations S4, we estimated the maximum value of $\Delta\chi$ to be approximately 2.2×10^{-20}

JT^{-2}.

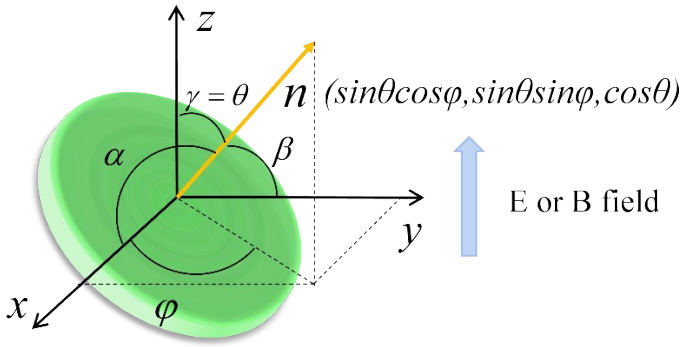

Figure S1. Sketch of the nanosheet coordinate and the measurement system applied in the simulation model. To evaluate the alignment of nanosheets under external fields, a Boltzmann distribution model was constructed[5], including the particle coordinate (a, b, and c axes) for individual nanosheets and a measurement coordinate (*x*, *y,* and *z* axes) for the birefringence cell. Here, the nanosheet's position is represented by the directional cosine of the normal *n*, yielding

$$cos\alpha = sin\theta cos\varphi, cos\beta = sin\theta sin\varphi, cos\gamma = cos\theta \quad \text{(S5)}$$

Where θ and φ are the Euler angles characterizing the relationship between the particle coordinates and the measurement coordinate system. Thus, we can obtain the orientation distribution function of the particle using the Boltzmann distribution, denoted as

$$f(\theta,\varphi) = exp(-\frac{U(\theta,\varphi)}{kT}) \Big/ \int exp(-\frac{U(\theta,\varphi)}{kT}) sin\theta d\theta d\varphi = exp(-\frac{U(\theta,\varphi)}{kT}) \Big/ N \quad \text{(S6)}$$

Here, $U(\theta, \varphi)$ represents the potential energy distribution, which involves the electric polarizability α_i and magnetic susceptibility χ_i in three directions.

For electric field-induced alignment simulation, note that the size difference in the lateral directions is rather small, and the polarization can be considered proportional to the size. As a result, a disk model is used to simplify the system with

$$\alpha_a = \alpha_b = \alpha \tag{S7}$$

Thus, the polarization anisotropy of the nanosheet is defined as

$$\Delta\alpha = -(\alpha - \alpha_c) \tag{S8}$$

As a result, the potential energy distribution under the electric field is expressed as

$$U_E(\theta,\varphi) = -(1/2)\left(\alpha sin^2\theta cos^2\varphi + \alpha sin^2\theta sin^2\varphi + \alpha_c cos^2\theta\right)\varepsilon_0 E^2 \tag{S9}$$

Using Equations S6 and S9, the orientation distribution function is obtained as

$$f_E(\theta,\varphi) = \frac{1}{N} exp[\left(\alpha sin^2\theta cos^2\varphi + \alpha sin^2\theta sin^2\varphi + \alpha_c cos^2\theta\right)\varepsilon_0 E^2/2kT] \tag{S10}$$

Then the order parameter S is expressed using the orientation distribution function as

$$S = \frac{\int_0^{2\pi}\int_0^{\pi} f(\theta,\varphi)P_2(cos\theta)sin\theta d\theta d\varphi}{\int_0^{2\pi}\int_0^{\pi} f(\theta,\varphi)sin\theta d\theta d\varphi} \tag{S11}$$

where the second-order Legendre polynomial $P_2(\cos\theta)$ can be expressed as $1/2(3\cos^2\theta\text{-}1)$. The birefringence can be expressed as

$$\Delta n = n_z - n_x = (\langle n\rangle + 2\Delta n_{sat}\varphi S/3) - (\langle n\rangle - \Delta n_{sat}\varphi S/3) = \Delta n_{sat}\varphi S \tag{S12}$$

Here, we obtain $\Delta n_{sat}\varphi$ by extrapolation using $1/E^2$. For 0.1-0.4 wt% 2D LC, the $\Delta n_{sat}\varphi$ was estimated to be 5×10^{-5}, 8×10^{-5}, 1.4×10^{-4}, 1×10^{-4}, respectively. At the same time, the order

parameter S was calculated using the obtained $\Delta\alpha$ and Equation S9-S11. Using the $\Delta n_{sat}\varphi$ for various concentrations and the order parameter S at different field strengths, the simulated curves in **Figure 2b** can be obtained.

For magnetic field-induced alignment simulation, according to Uyeda's method to calculate the diamagnetic anisotropies of nanosheets[6], the magnetic susceptibility of the long axis (χ_a) and the normal direction (χ_c) is approximately equal, whereas they differ significantly from χ_b. This indicates that the lateral plane may be the magnetic easy plane. However, considering the large aspect ratio of the nanosheet, the demagnetization energy cannot be neglected[7]. The demagnetization energy is closely related to the shape anisotropy, expressed as

$$U_{de\_i} = -(1/2)N_i\chi_i^2B^2 \tag{S13}$$

Of which N_i (i=a, b, c) is the demagnetization coefficient in the i direction. Based on the aspect ratio, the demagnetization coefficient is calculated to be N_a=0.00008, N_b=0.00008, and N_c=0.99984. As a result, $U_{de\_a} \approx U_{de\_b} \gg U_{de\_c}$, and the normal direction n is finally determined as the easy axis[8, 9]. After taking the demagnetization parameter in to account, the magnetic susceptibility $\chi_a^* \approx \chi_b^* \ll \chi_c^* < 0$, take $\chi_a^* = \chi_b^* = \chi$ and $\chi_c^* = \chi_c$, then we obtain $\chi_c/\chi \approx 0.0001$. Similar to Equation S9, the potential energy in the magnetic field is

$$U_B(\theta,\varphi) = -(1/2)\left(\chi sin^2\theta cos^2\varphi + \chi sin^2\theta sin^2\varphi + \chi_c cos^2\theta\right)B^2 \tag{S14}$$

Then the orientation distribution function is obtained by substitution

$$f_B(\theta,\varphi) = \frac{1}{N} exp[\left(\chi sin^2\theta cos^2\varphi + \chi sin^2\theta sin^2\varphi + \chi_c cos^2\theta\right)B^2/2kT] \tag{S15}$$

As the concentration increased, the magnetic birefringence curves exhibited variations. The calculated Δχ increased to fit the curves among different concentrations. $\Delta\chi$ and $\Delta n_{sat}\varphi$ are shown in table S1, respectively. By using Equations S11 and S15 along with $\Delta\chi$ in **Table S1**, we can obtain the simulated order parameter S, which, when combined with $\Delta n_{sat}\varphi$ in **Table S1**, ultimately produces the simulated magneto-optic birefringence curves in **Figure 2d**.

Table S1. The calculated $\Delta\chi$ and $\Delta n_{sat}\varphi$ of concentrations ranging from 0.1 wt% to 0.8 wt%.

	0.1 wt%	0.2 wt%	0.3 wt%	0.4 wt%	0.6 wt%	0.8 wt%
$\Delta\chi(JT^{-2})$	3.39×10^{-22}	9.89×10^{-22}	5.95×10^{-21}	7.92×10^{-21}	1.86×10^{-20}	2.22×10^{-20}
$\Delta n_{sat}\varphi$	3.04×10^{-5}	6.59×10^{-5}	7.93×10^{-5}	1.08×10^{-4}	1.68×10^{-4}	2.21×10^{-4}

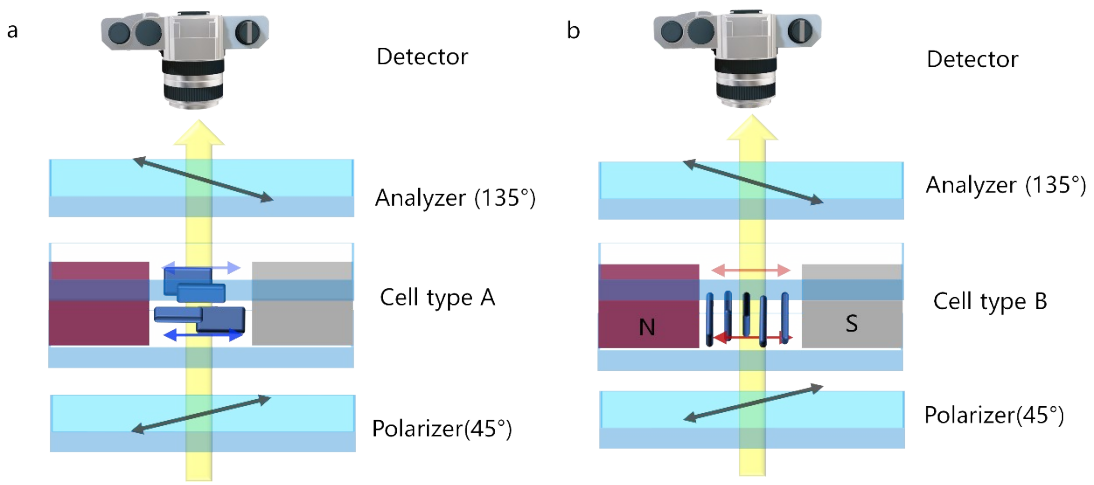

Figure S2. The experimental setup for birefringence measurement. (a) measurement of the electric-field-induced birefringence using crossed polarizers and a detector. (b) measurement of the magnetic-field-induced birefringence using crossed polarizers and a detector.

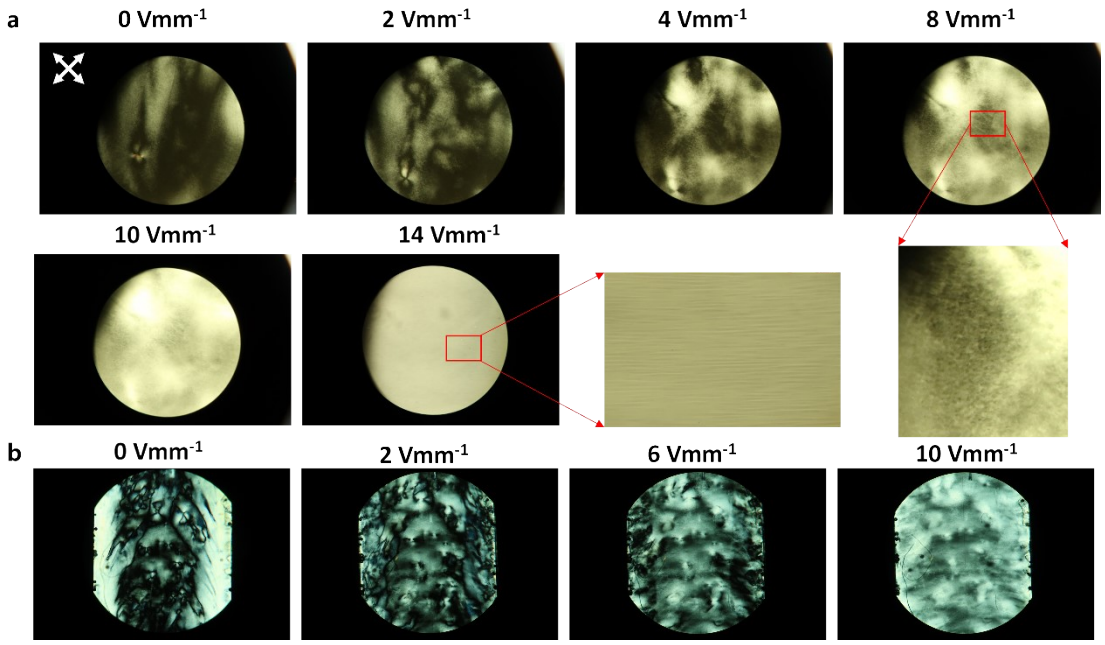

Figure S3. Images of POM pattern in the electric fields. (a) as the voltage increases, the birefringence pattern of 0.3 wt% 2D LC changes from dark to light, finally exhibiting the Williams domain. (b) an intrinsic birefringence was shown after injecting the 0.6 wt% LC into the cell, which was erased when the voltage was turned on.

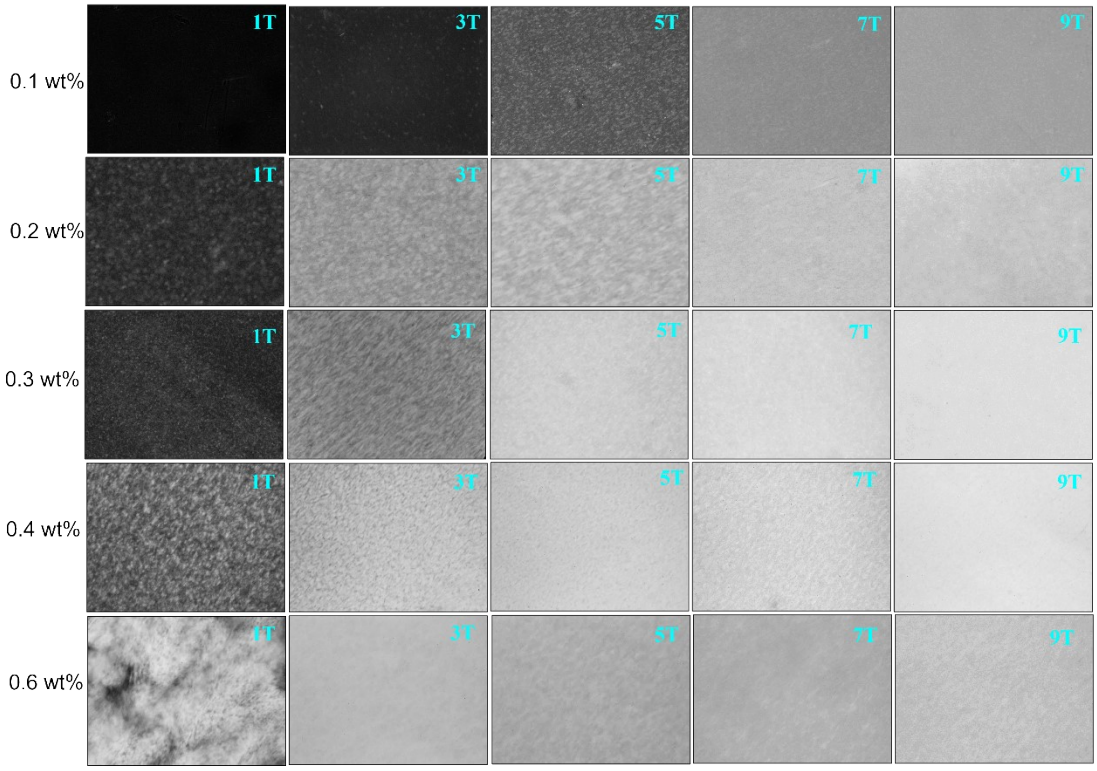

Figure S4. Images of POM pattern at varying concentrations in a magnetic field. The birefringent domains, which are bright and distributed in blocks, can be easily identified in low field strengths. Meanwhile, the macroscopic alignment was enhanced in situ for 0.4 wt% and 0.6 wt% 2D LC.

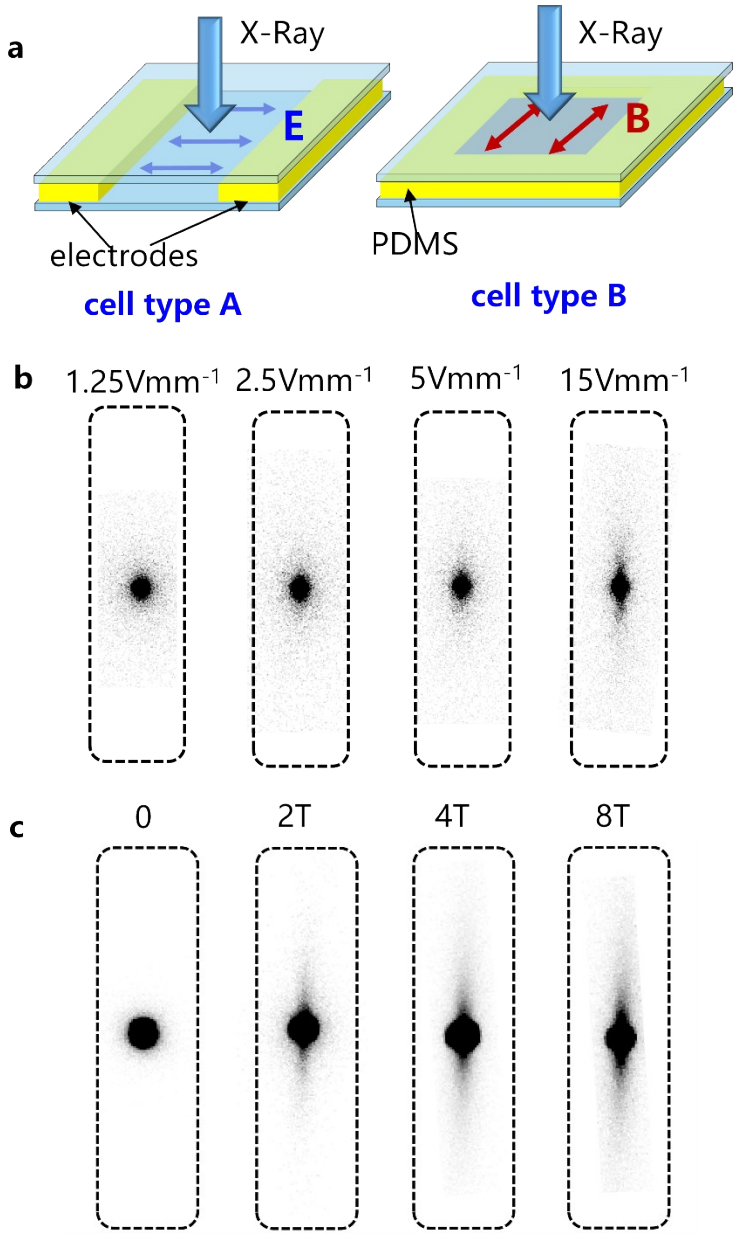

Figure S5. SAXS patterns of aligned 0.3 wt% 2D LC in electric and magnetic fields, respectively. (a) the fabricated cells for SAXS measurements, and the coordinate system. The electric-field cell consists of a bottom glass substrate, aluminum electrodes in the middle layer, and a top encapsulating glass cover. The bottom glass substrate has dimensions of 30 mm in length, 15 mm in width, and 1 mm in thickness. Two aluminum electrodes, each measuring 10 mm × 15 mm × 1.2 mm, are attached at the central region of the glass substrate. The groove formed between the electrodes and the glass substrate is filled with the nanosheet dispersion. Finally, the cell is sealed with a top glass substrate identical to the bottom one. The magnetic-field cell consists of top and

bottom glass substrates with a PDMS spacer layer in between. The glass substrates have dimensions of 20 mm × 20 mm × 1 mm (length × width × thickness). The PDMS spacer has an outer lateral dimension of 20 mm × 20 mm and an inner opening of 15 mm × 15 mm, with a thickness of 3 mm. The internal cavity is filled with the nanosheet dispersion, corresponding to a volume of 15×15×3 mm^3. (b) the SAXS patterns of 0.3 wt% 2D LC aligned by the electric field. The profile changed from a circular to an elliptical shape, indicating that the normal direction of the 2D LC is likely to be aligned perpendicular to the electric field[10]. (c), the SAXS patterns of 0.3 wt% 2D LC aligned by the magnetic field, indicating a normal direction parallel to the magnetic field.

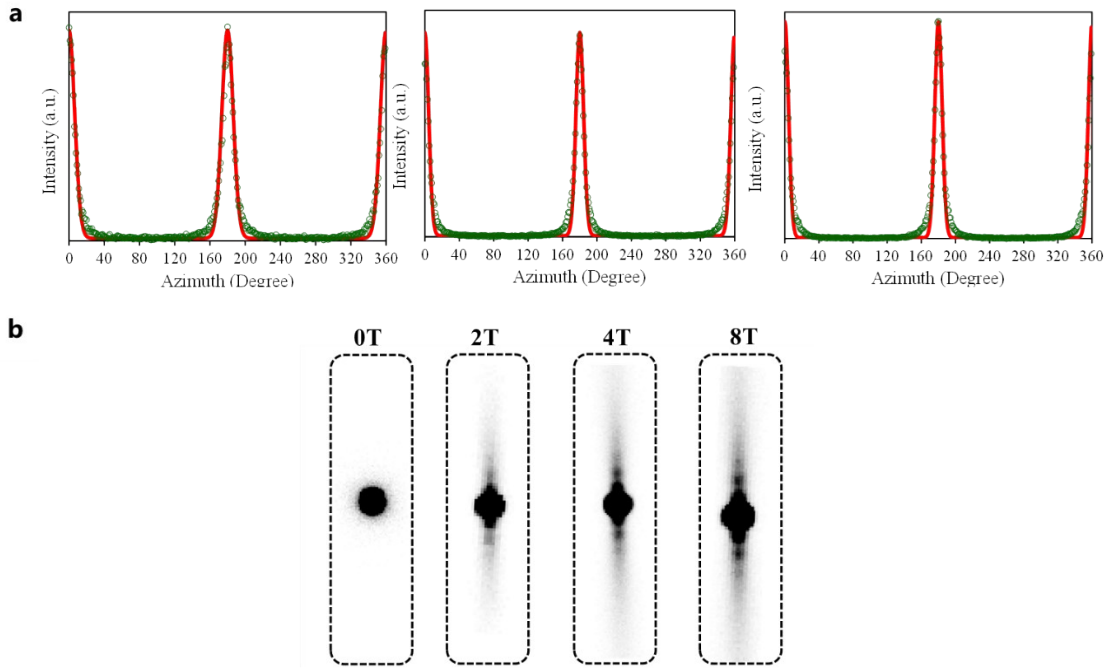

Figure S6. SAXS patterns of aligned 0.6 wt% 2D LC in magnetic fields. (a) the azimuthal plots of 2D LC under 2T, 4T, and 8T magnetic fields. (b) the SAXS patterns of 0.6 wt% 2D LC aligned using magnetic fields. The profile from 2T to 8T had scattering peaks up to the (300) face, corresponding to a constant interflake spacing[11].

REFERENCES

(1) Dozov, I.; Paineau, E.; Davidson, P.; Antonova, K.; Baravian, C.; Bihannic, I.; Michot, L. J., Electric-field-induced perfect anti-nematic order in isotropic aqueous suspensions of a natural beidellite clay. *J Phys Chem B* **2011,** *115* (24), 7751-65.
(2) van der Beek, D.; Petukhov, A. V.; Davidson, P.; Ferre, J.; Jamet, J. P.; Wensink, H. H.; Vroege, G. J.; Bras, W.; Lekkerkerker, H. N., Magnetic-field-induced orientational order in the isotropic phase of hard colloidal platelets. *Phys Rev E Stat Nonlin Soft Matter Phys* **2006,** *73* (4 Pt 1), 041402.
(3) Ding, B.; Kuang, W.; Pan, Y.; Grigorieva, I. V.; Geim, A. K.; Liu, B.; Cheng, H. M., Giant magneto-birefringence effect and tuneable colouration of 2D crystal suspensions. *Nat Commun* **2020,** *11* (1), 3725.
(4) Shen, T. Z.; Hong, S. H.; Song, J. K., Electro-optical switching of graphene oxide liquid crystals with an extremely large Kerr coefficient. *Nat Mater* **2014,** *13* (4), 394-9.
(5) Hong, S. H.; Shen, T. Z.; Song, J. K., Dual-field-induced biaxial nematic ordering of two-dimensional nanoparticles and enhancement of interparticle interactions. *Phys Rev E* **2019,** *100* (2-1), 020701.
(6) Uyeda, C., Diamagnetic anisotropies of oxide minerals. *Physics and Chemistry of Minerals* **1993,** *20* (2), 77-81.
(7) Liu, M.; Ishida, Y.; Ebina, Y.; Sasaki, T.; Hikima, T.; Takata, M.; Aida, T., An anisotropic hydrogel with electrostatic repulsion between cofacially aligned nanosheets. *Nature* **2015,** *517* (7532), 68-72.
(8) Wu, L.; Ohtani, M.; Takata, M.; Saeki, A.; Seki, S.; Ishida, Y.; Aida, T., Magnetically induced anisotropic orientation of graphene oxide locked by in situ hydrogelation. *ACS Nano* **2014,** *8* (5), 4640-9.
(9) Wang, X.; Li, X.; Aya, S.; Araoka, F.; Ishida, Y.; Kikkawa, A.; Kriener, M.; Taguchi, Y.; Ebina, Y.; Sasaki, T.; Koshiya, S.; Kimoto, K.; Aida, T., Reversible Switching of the Magnetic Orientation of Titanate Nanosheets by Photochemical Reduction and Autoxidation. *J Am Chem Soc* **2018,** *140* (48), 16396-16401.
(10) Nie, Y. J.; Huang, G. S.; Qu, L. L.; Wang, X. A.; Weng, G. S.; Wu, J. R., New insights into thermodynamic description of strain-induced crystallization of peroxide cross-linked natural rubber filled with clay by tube model. *Polymer* **2011,** *52* (14), 3234-3242.
(11) Shintate, M.; Inadomi, T.; Yamamoto, S.; Kuboyama, Y.; Ohsedo, Y.; Arimura, T.; Nakazumi, T.; Hara, Y.; Miyamoto, N., Anisotropic Self-Oscillating Reaction in Liquid Crystalline Nanosheet Hydrogels. *J Phys Chem B* **2018,** *122* (11), 2957-2961.